The Seventh International Colloquium on Bluff Body Aerodynamics and Applications (BBAA7)
Shanghai, China; September 2-6, 2012

On the characterization of wind profiles generated by road traffic

Salvadori S. [a], Morbiato T. [b], Mattana A. [a], Fusto E. [b]

[a] *CRIACIV, University of Firenze, via di S. Marta, 3 – Florence, Italy*
[b] *ICEA Dept., University of Padova, via Marzolo, 3 – Padova, Italy*

ABSTRACT: This paper analyses the flow field and the power wasted by a heavy-duty truck of modified GTS standard shape (equivalent to GCM class 8). Computational fluid dynamics has been used to analyze truck models at cruise conditions. The selected test matrix includes the study of an isolated truck and of a train of two and three trucks to evidence interaction effects. For each case three different velocities have been considered. The numerical campaign is able to quantify the drag coefficient distribution, the losses generated on the roof by viscous phenomena and the changes in velocity distributions. An in-situ experimental campaign is also settled in the truck lane of Venice highway using ultrasonic anemometers and video cameras set on the same measurement frame. Non-dimensional velocity distributions along the vehicle confirm that the height of the separation bubble is dependent on the number of trucks.

KEYWORDS: Truck, Drag Coefficient, Power Losses, CFD, Ultrasonic Anemometer

1 ACKNOWLEDGEMENTS

The *TrEo* group would like to acknowledge the funding institution “Progetti di Eccellenza - Fondazione Cassa di Risparmio di Padova e Rovigo” for supporting the proposed research. The Scientific Board, composed of Prof. R. Vitaliani of the University of Padova and Prof. C. Borri of the University of Firenze, is also acknowledged.

2 INTRODUCTION

The effects induced by the transit of heavy-duty trucks have been widely addressed in the open literature. Experimental results mainly derive from works on road sign resistance, some insights being captured with accuracy and wealth of details. From a numerical point of view, much information are provided on the turbulence modeling effects, ranging from simple Reynolds Averaged Navier-Stokes (RANS) calculations to Large Eddy Simulation (LES), and on the unsteady flow field occurring in the rear part of the vehicles. Research on the premature failure of the USA type cantilevered traffic signal structures and deficiencies in the UK design standards on road signs gave the opportunity to obtain details about what happens in the proximity of a passing truck. A review of the work done in the field of induced gust loads on cantilevered structures can be found in the work of Albert [1]. The works by Cali and Covert [2] and Quinn et al. [3] are of interest for the reliability and size of their experimental databases. Cali and Covert [2] performed experimental measurements of the loads on a 1:30 scale model of an overhead highway sign with varying sign height and truck length, speed and shape. They described in detail the interaction between a road sign and a passing truck through the force coefficient evaluated on the sign itself. Vehicle passing was divided into four phases that always occur, the last one depending on the dimension of the truck only. Quinn et al. [3] studied the phenomena responsible for the vehicle-

induced loads. Their experimental apparatus was used to evaluate longitudinal loads on real signs of different size and shape placed at the side of the carriageways of two different roads. They demonstrated that the load induced by the truck passing is due to the pressure field related to the potential flow region of the vehicle slipstream, rather than a significant vehicle induced gust effect. Considering the evaluation of the drag coefficient of moving trucks, the works of Ougburn et al. [4], Storms et al. [5], Wood and Bauer [6] and Diebler and Smith [7] provide detailed information on the power wasted for aerodynamic effects. From a numerical point of view, Salari et al. [8], Roy et al. [9] and Veluri et al. [10] demonstrated that the RANS approach is able to predict pressure fields on trucks surfaces except for the base region. It is also concluded that although in the latter zone pressure field and flow structure predictions do not match with experimental data, an accurate prediction of the vehicle drag depends on the turbulence model only. Veluri et al. [10] quantified that error in around 5% when using k-ε or k-ω models, while higher discrepancies have been individuated when using Spalart-Allmaras or SST. The latter results have also been confirmed by the RANS simulations performed by Pointer [11], with an improved performance of SST model. Hyams et al. [12] presented a detailed study using RANS and Unsteady RANS (URANS) approaches. There are no relevant differences between the steady and the time-averaged data, neither in terms of pressure distributions along surfaces nor in terms of drag coefficient evaluation. There is also a good agreement with experimental data, except for the base region where an improved approach seems to be necessary. The work of Maddox et al. [13] deals with the comparison between purely RANS prediction and Detached Eddy Simulation (DES), both working with the Spalart-Allmaras turbulence model. They demonstrated that the a RANS approach is equivalent to DES except for the evaluation of the base region, where the recirculation flow is well captured by the resolution of large eddies. A detailed description of the flow field occurring in the base region has been proposed by Krajnović and Davidson [14] using LES on a simplified geometry. A more realistic vehicle is investigated with LES by Östh [15]. Although the accuracy of LES is very high, the computational load is unacceptable while the discrepancy between the experimental and the numerical drag coefficients is of the same order of magnitude found for a simple RANS calculation with a k-ε closure. Although there is a wide literature on the selected topic, information on the energy transfer due to the skin-friction on the roof of trucks as well as a detailed description of the flow field generated by the truck movement is missing. The present paper studies this topic both from an experimental and a numerical point of view. Results are discussed also considering the literature data and an insight on the separated boundary layer occurring on the trailer roof is presented.

3 DESCRIPTION OF THE PROPOSED APPROACH

The power wasting related to the skin-friction effect occurring on the roof of a truck has been estimated by means of a mono-dimensional approach based on the data available in the open literature for a scaled GTS. Once that activity has been concluded, the analysis of the induced pressure and velocity fields generated by trucks has been performed considering both an experimental and a numerical approach. The latter has been used to study a controlled environment where the truck passing effect could be isolated and the truck-truck interaction studied for typical cruise conditions. Furthermore, the numerical results have been used to quantify the amount of power that is transferred to the turbulent boundary layer, thus validating the simplified approach. The experimental approach demonstrated the accuracy of the numerical analysis and provided further information on the realistic situation, including the individuation of velocity peaks as well as the presence of long lines of trucks over the investigated area.

3.1 *The numerical approach*

Computational Fluid Dynamics (CFD) allows for detailed analysis of complex geometries. Incompressible, steady simulations have been performed on a specific vehicle model, which is defined to represent the typical European truck. The inherent complexity of the research demands for simplified approaches, and then a 2D numerical campaign has been completed using the commercial code ANSYS Fluent®. Calculations have been performed in the relative frame of reference and are second order accurate in space. Turbulence is modeled using the two equations k-ε model with standard wall functions. Simulations have been performed considering up to three trucks to study the aerodynamic effects. A total amount of 18 simulations have been performed, as reported in Table 1.

Table 1. Test matrix

Section	Vehicles	Distance (m)	Domain H x L (m2)	Number of elements	Speed (km/h)
W,NW	1 truck	0	100 x 120	~250,000	90 ,100 ,110
	2 truck	10	100 x 148	~300,000	90 ,100 ,110
	3 truck	10, 10	100 x 176	~360,000	90 ,100 ,110

A vehicle with a shape like that of the GTS has been considered, including the tractor-trailer gap. The computational domains represent both a section at the centerline of the truck (called No-Wheels, NW) and a section that includes the wheels (identified by W, Wheels). Minor details are neglected since the main contribution to the wasted power and air displacement comes from the bulk of the vehicle. Computational domains are discretized with an unstructured mesh where both triangular and quadrilateral elements are used (Figure 1a). Special attention has been paid to the discretization of the gap between the trucks and the lower region of the domain, where the re-circulating phenomena should occur (Figure 1b). The top of the domain has been modeled using a far-field condition where the total pressure is uniform and the flow is undisturbed. Those dimensions provide a vertical blockage of approximately 5% that will introduce an overshoot of velocity in the near-truck region. That effect will be considered while discussing the obtained results. For each investigated case, the last truck has been maintained at a constant distance from the outlet section to keep unchanged the reference pressure value for the pressure coefficient calculation.

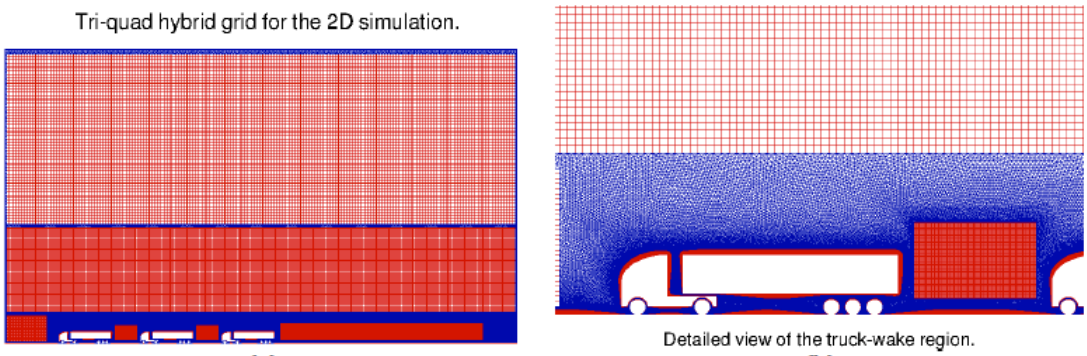

Figure 1. Computational grid of the three-trucks case: full domain (a) and wake region (b)

3.2 *The experimental apparatus*

The aim of the experimental campaign is to reconstruct the wind velocity profile on the top of truck in the lane axis, with an approach taking into account three-dimensional components attributed both to viscous fluid transportation properties and to interaction between pressure wave, rear wake, and vehicles gap in high traffic density. To this aim, the Venice link highway offers steel bridge frames of 200mm squared hollow sections bearing the traffic messages led panels and pictograms. To prevent interferences in wind measurements, at the chosen frame the 2.5m high panel in the instruments approaching direction has been removed, and substituted by a low solidity 50x50mm net handrail only 2mm thick. Each lane is instrumented with 3 ultrasonic triaxial anemometers (USA) 40 Hz hi-freq. sampling, cantilevered > 2m from frame and placed at 5.50 m minimum headroom from road, at 6.50 m and at 7.50 m. The vertical alignment is avoided for two adjacent instruments in order to maximize mutual distance, and achieve not-interfering condition according to the ILAC MRA certified instrument. Another tri-axial USA is placed at 12 m height, sampled 8 Hz and interpolated to 40 Hz in order to get an ambient wind survey to calibrate traffic wind from aerodynamic losses. To correctly estimate interactions in high traffic density, an image tracking system is integrated with synchronous wind speed sampling. A couple of video cameras are set on the top of the measurement frame bridging the roadways. While the USA network is acquiring the environmental wind speed and the vehicle induced wind gusts, the cameras extract the size and speed of those vehicles, which generated the perturbations exciting the measurement system. Once truck geometry, speed and trajectory are estimated with a stereo tracking algorithm, a statistics is made on the collected data and estimates. A typical anemometry set for a single lane 3.5m wide is illustrated in Figure 2.

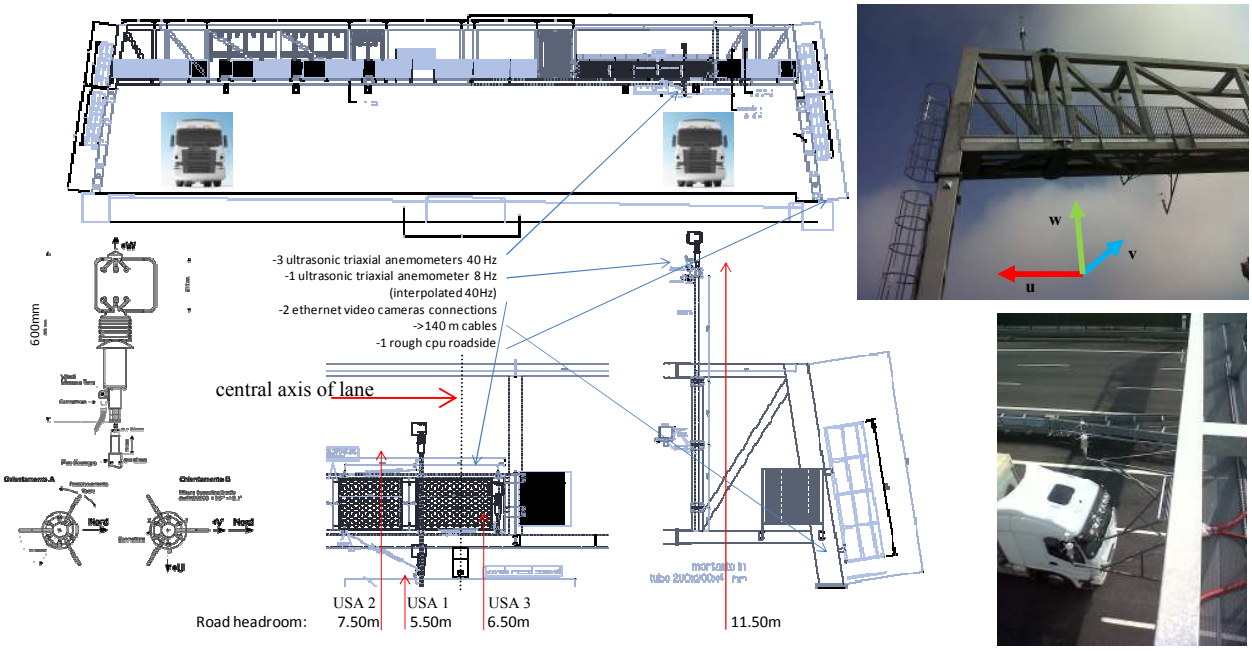

Figure 2. Experimental apparatus on the highway for a typical single-lane one directional set-up: the wind speed co-ordinates system and the USA numbering conventions are indicated. Note that USAs are placed symmetrically respect to central axis of the lane (1,2 one side, 3 other side)

4 NUMERICAL ANALYSIS OF LOSSES AND OF THE PRESSURE/VELOCITY PROFILES

The aim of the numerical activity is to investigate the pressure and velocity profiles generated by a moving truck and to quantify the amount of power lost by skin-friction on the roof of the truck itself. For the latter analysis the data available in the open literature for a Class-8 tractor-trailer are used. According to Ougburn et al. [4], the engine of a truck moving at 100km/h provides an amount of power of approximately 132kW. The 48% of that amount, around 63kW, is wasted for aerodynamic effects that are accounted for when the drag coefficient (Cd) is evaluated. The use of CFD will provide detailed information on the Cd distribution and then on the distribution of losses.

4.1 *Evaluation of the power losses related to the trailer roof skin-friction*

A preliminary analysis based on the assumption that the trailer roof can be treated as a flat plate will provide an estimation of the energetic content of the developing turbulent boundary layer. The skin-friction values for the full-scale GTS case can be estimated considering the drag coefficient values proposed by Storms et al. [5] for a 1/8-scaled model. Dynamic similarity is considered to scale the truck velocity and maintain the same Reynolds numbers. Being the flow incompressible and maintaining the flow viscosity unaltered, the ratio between the model and the full-scale truck velocities is 8. As a consequence, for a truck moving at 100km/h a Re of 4.8E+06 must be considered. According to Storms et al. [5] the total drag coefficient is almost constant for Re number higher than 1E+06, and then a constant value can be assumed. A C_d value of 0.249 is calculated integrating on the trailer the experimental skin friction distribution for the GTS model as found in Storms et al. [5] and depicted in Figure 3 with red squares (the leading edge starting at x/w = 2), together with its interpolation curve (in blue) and the theoretical turbulent flat plate prediction for a Reynolds number of 2.E+06 (dashed black).

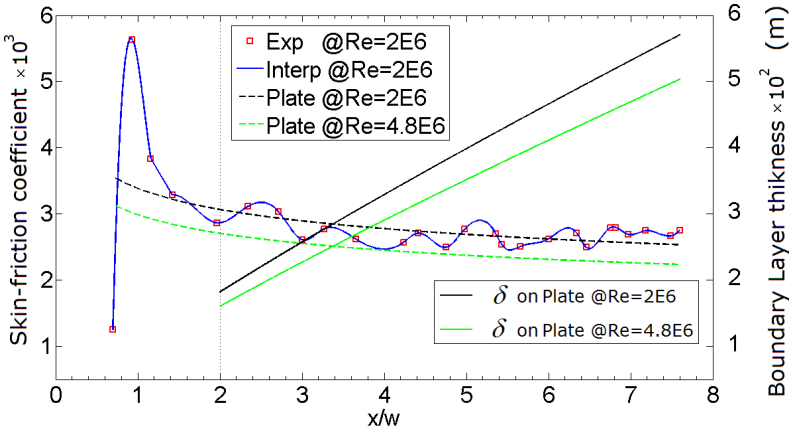

Figure 3. Skin friction and boundary layer thickness distribution for the GTS model at 2.E+06 and 4.8E+06 Reynolds numbers

The evaluation of the skin-friction drag can be performed considering a flat plate subject to the selected conditions. The skin-friction distribution at the needed Reynolds number of 4.8E+06 can be evaluated using Equation 1 (dashed-green curve in Figure 5).

$$c_f = \frac{0.034}{\mathrm{Re}_x^{1/7}} \tag{1}$$

The experimental results obtained on the 1/8-scaled model are compared with the data obtained for a full-scale flat plate at 100km/h in Table 1. Subscript $_c$ stands for "corrected", the latter being used to indicate the GTS total drag coefficient accounting also for the wheels (+0.1, Wood and Bauer [6]), the tractor-trailer gap (+0.1, Wood and Bauer [6]) and the under-body (+0.07, deduced from Diebler and Smith [7]) contributions. It can be evidenced that the $C_{df,roof}$ value obtained for a full-scale truck leads to an underestimated value of total drag contribution (around -13.8%) with respect to the experimental data.

Table 2. Comparison between GTS drag values for different Re numbers

Case	Re	C_d	$C_{d,c}$	$C_{df,roof}$	$C_{df,roof}/C_{d,c}$ (%)
Experimental	2.E+06	0.249	0.519	0.0101	1.95
Flat-plate (full scale)	4.8E+06	0.249	0.519	0.0087	1.68

As suggested by White [16], it is possible to calculate the boundary layer thickness on the roof of the GTS at full-scale. Assuming for simplicity that the boundary layer can be modeled using a power law as suggested by Prandtl, its growth is reported in Figure 5 for Re = 2.E+06 (black curve) and for Re = 4.8E+06 (green curve). Similar evaluations could be performed starting from the data obtained by Storms et al. [5] and varying the Reynolds number to mimic different truck velocities. Values of the boundary layer thickness with varying speed at the leading edge (LE), at the middle point (MP) and at the trailing edge (TE) of the trailer for the full scale GTS are shown in Table 3.

Table 3. Boundary layer thickness at the trailer's roof and skin-friction power losses computed using an approximate approach based on the full-scale flat-plate assumption for a GTS model

Speed	δ (cm)			$P_{f,roof}$
(km/h)	LE	MP	TE	(kW)
90	13.0	27.6	40.9	0.91
100	12.8	27.2	40.3	1.23
110	12.7	26.8	39.7	1.61

Once the value of the skin-friction drag is available it is also possible to evaluate the power transferred to the boundary layers using Equation 2:

$$P_{f,roof} = \frac{1}{2}\rho_r U_r^3 A_r C_{df,roof} \tag{2}$$

In that equation U_r is the vehicle's speed, ρ_r is the air density at ambient conditions and A_r is the projected area of the truck as seen from the main-flow. Although skin-friction coefficients are made non-dimensional basing on the wetted area, the truck frontal area is now used for homogeneity with the drag coefficient definition. The truck power transferred to the roof boundary layer is reported in Table 2. As can be seen, at 100 km/h the power losses generated by the skin-friction on the roof of the trailer amounts to 1.23kW, which is around 1% of the total power produced by the engine and around 2% of the aerodynamic losses. The obtained results demonstrate that the skin-friction on the trailer roof provides a negligible contribution to the net aerodynamic

losses. It is worth noting that these flat-plate predictions assume implicitly that the boundary layer transition locates at the same point of the experimental case, while increasing the Reynolds number implies that transition occurs somewhere before and that boundary layer becomes thinner. Therefore, numerical simulations are necessary to focus into the flow field around the truck, where the prevailing losses are spent to displace the fluid from the vehicle way.

4.2 *CFD of the selected cases*

As already pointed out, the RANS approach is used to study a truck moving in a leveled and windless highway. Several simulations have been performed to gain general rules for the phenomena involved, also considering the effects of trailing trucks.

4.2.1 *2D results*

Since one of the objectives of the activity is to evaluate the height of the recirculating boundary layer over the trucks, comparisons are always performed considering the last truck of the row. Only the results obtained for 100km/h will be shown, being negligible the differences between the non-dimensional profiles obtained for the other cases. Furthermore, there are no relevant differences between the case with wheels and the case that mimic the central section of a real truck, and then only the case with wheels will be shown. The data obtained for the no-wheels case will be used in the evaluation of the total drag coefficient. The non-dimensional absolute axial velocity profiles are shown in Figure 4 and Figure 5-a for the case with wheels. Velocity profiles are depicted for three axial positions: the leading edge (LE) and trailing edge (TE) of the trailer and its mid-point (MP). The absolute axial component of the velocity is divided by the truck velocity U_0; the distance from the road is divided by the height of the truck. Dashed lines indicate the minimum height where obstacles position is allowed in European countries. For each profile, the Y/H position that corresponds to the $V_x/U_0 = 0$ value can be considered as the height where the separation bubble ends. As can be observed, the highest value of the separation bubble height, reached near the TE, is almost negligible when considering a single truck moving along the lane, being Y/H around 1.1 at the TE for $V_x = 0$. A different behavior can be observed looking at the last truck of a row of two or three, being the Y/H value correspondent to the bubble closure always equal to or higher than 1.2. In fact, at the LE the Y/H value reaches values of 1.3 for a row of three (Figure 4-a) and maintained over 1.25 also at MP (Figure 4-b) and TE (Figure 5-a). The latter result indicates that the separation bubble never reattach on the third truck when considering a row of three, which is a conditions that often occurs.

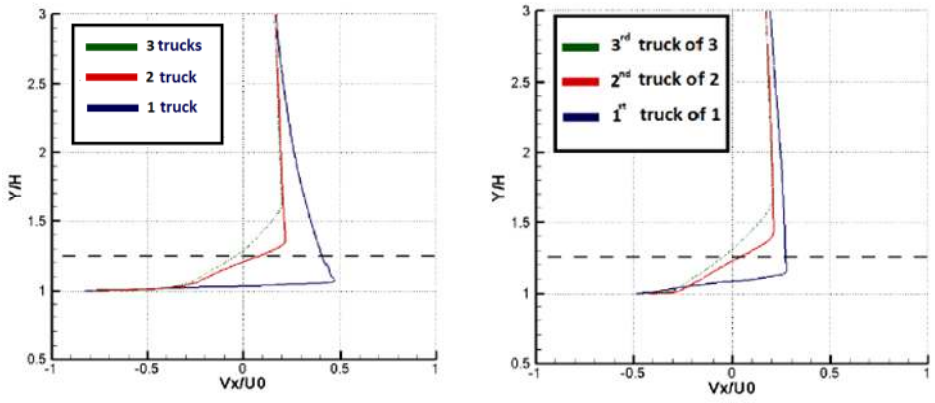

(a) 100km/h @LE, W (b) 100km/h @MP, W

Figure 4. Leading edge and mid-point profiles for wheel (W) case at 100km/h

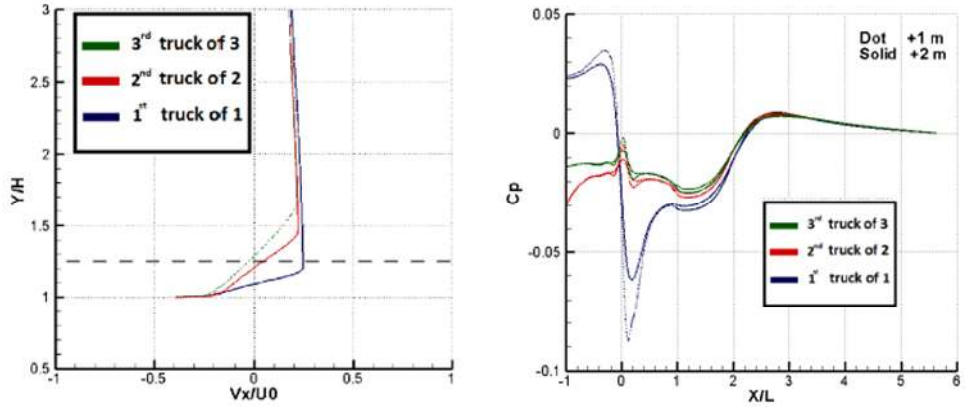

(a) 100km/h @TE, W (b) 100km/h, W

Figure 5. Trailing edge profiles for wheel (W) case and pressure coefficient distribution at 100km/h

That differences between the flow fields are also evidenced by the absolute velocity field near LE and TE for the cited cases, as shown using the same velocity scales in Figure 6 and Figure 7. The flow separation is depicted with a red line (that indicates $V_x = 0$) in Figure 6-a near the LE and in Figure 7-a near the TE of the first truck. As can be seen, the effect induced by the skin-friction on the shear layer is limited and the flow velocity turns to 0 not far from the trailer roof. Looking at the velocity field generated by the third truck (Figure 6-b and Figure 7-b), it is clearly visible that the flow is almost constant and moves in the direction of the truck, which means that the flow is completely separated. It can be supposed that the longest the truck row will be, the higher will be the separated region. It is worth mentioning that the Y/H value where an undisturbed flow can be individuated is at least 1.15 for the first truck at MP (Figure 5-a). Considering a value of 4m for H, which is the value chosen in this study as representative of European trucks, the height of the boundary layer is at least 60cm instead of the 40cm predicted for 100km/h by the flat plate approach (Table 3). The latter neglect the presence of flow separation, which is the driving phenomenon when studying trucks aerodynamics. It must be observed that in a 2D simulation, the blockage effect of the truck height is a crucial parameter and that the velocity modules are slightly overestimated. Nevertheless, the observed trends will not change in a realistic environment, as demonstrated by the experimental campaign described below.

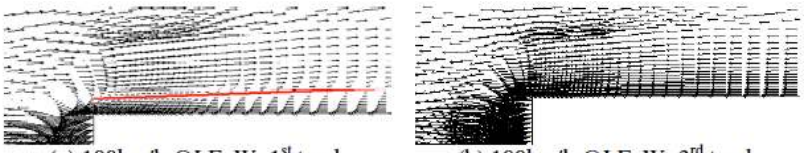

(a) 100km/h @LE, W, 1st truck (b) 100km/h @LE, W, 3rd truck

Figure 6 Leading edge profiles for wheel case at 100km/h

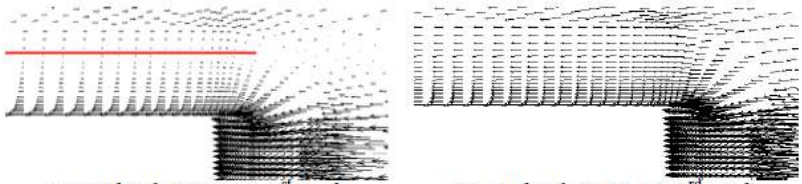

(a) 100km/h @TE, W, 1st truck (a) 100km/h @TE, W, 3rd truck

Figure 7 Trailing edge profiles for wheel case at 100km/h

A final comment can be done on the pressure fields associated to the already discussed velocity profiles. In Figure 5-b the pressure coefficient C_p is reported for two different heights above the truck roof. As expected, the pressure fluctuation associated with the first truck is quite high (from +0.35 to -0.9) and the overall C_p trend is coherent with the description provided by Cali and Covert [2]. The subsequent trucks are subject to a smaller pressure drop that results in a smaller drag coefficient associated to the truck progress.

4.3 *C_d distribution*

The drag coefficients calculated using the data obtained from the numerical simulation of a single truck are shown in Table 4 for three different velocities. The C_d value is evaluated considering both the pressure (C_{dp}) and the skin-friction (C_{df}) effects. The relative contribution of the roof skin-friction to the total C_d can be compared with the data found in the open literature and from the flat plate approach (Table 2). It can be observed that the $C_{df,roof}/C_d$ value obtained for 100km/h is very similar to the experimental one (1.95%). That means that a 2D analysis is able to predict with reasonable accuracy the viscous drag effects also with a steady assumption, and that such kind of approach could be considered as a preliminary step in the truck shape optimization, prior to the use of accurate but demanding approaches as URANS or LES.

Table 4. Drag values calculated using both NW and W data

Speed (km/h)	C_{dp}	C_{df}	C_d	C_{df}/C_d (%)	$C_{df,roof}/C_d$ (%)
90	0.466	0.0172	0.483	3.50	1.79
100	0.464	0.0173	0.481	3.16	1.81
110	0.463	0.0168	0.432	3.47	1.80

5 EXPERIMENTAL TESTS ON A HIGHWAY

Vehicle-induced turbulence, hence the mark of the wind flow generated by road traffic, is highlighted via TKE turbulent kinetic energy:

$$e_i = \frac{1}{2}\left(\overline{u'^2_i} + \overline{v'^2_i} + \overline{w'^2_i}\right) \tag{3}$$

In particular, according to Kalthoff et al. [17], TKE difference between anemometer position lee and windward, normalized to wind speed u directed across highway, shows a strong correlation (R=0.77) with hourly traffic density of heavy duty vehicles circulating at a mean speed V=120 km/h. This is globally a sign of non-negligible energy along a non-ambient wind direction, due to highway traffic. Stemming from these global findings, the experimental campaign illustrated in Figure 2 goes further into the reconstruction of the wind profile due to heavy-duty traffic. A first signal processing gives the time domain results as presented in Figure 8. Mean ambient wind speed is evaluated each 10' and subtracted to obtain turbulent components (blue to green lines in Figure 8). The issue of filtering possible turbulent ambient wind speeds is addressed considering that atmospheric wind spectrum is generally characterized by a macro meteorological peak, followed by a spectral gap (10' to 60') and a micro meteorological peak (45"-50"). While single vehicle passages occur at sub 1" periods (gray bands in Figure 8), columns of trucks are also encountered collectively giving non negligible TKE during up to 50" periods: applying a multi-band filter to exclude both macro and micro atmospheric peaks is therefore not advisable, preferring a base band (random noise) Parks-McClellan FIR linear phase filter at 0.05 Hz cut-off (red line in Figure 8). It is worth noting from wind speed sign in Figure 8 that the flow moves in the direc-

tion of the truck and not opposite, as previously discussed and obtained via CFD. Finally, the peak detector fed with such a filtered signal, could detect the correct local maxima by looking for downward zero-crossings in the smoothed first derivative that exceeded a certain pre-determined minimum "slope threshold" at those points where signal exceeded a certain minimum "amplitude threshold", determining the coordinates (time instant and height), and approximate width of each peak by least-squares curve-fitting the top part of the peak (Oppenheim et al. [18]).

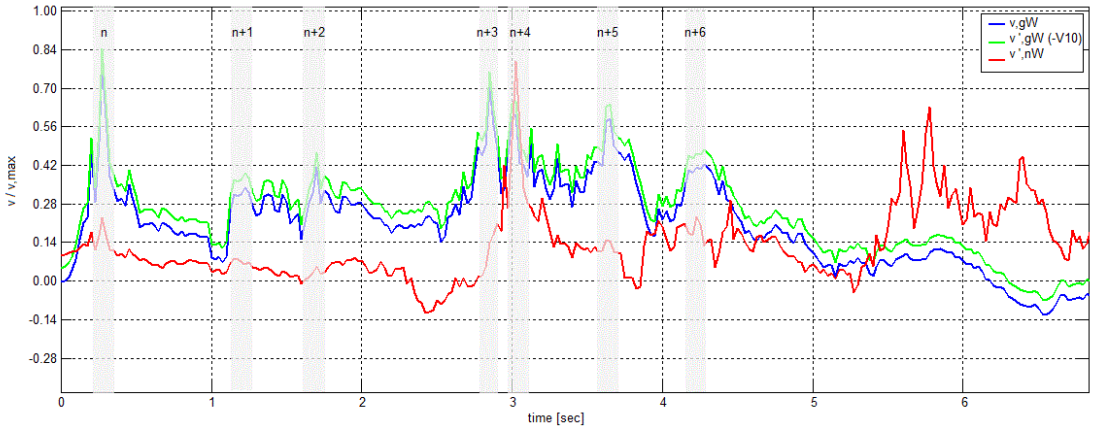

Figure 8 Sub-process n°6/12: 12h00 to 14h00: Time series of the normalized wind speed component directed along highway at 5.50m high USA: gross wind (blue), turbulent wind (green), turbulent filtered wind (red). Leading edge passages are also highlighted in gray bands.

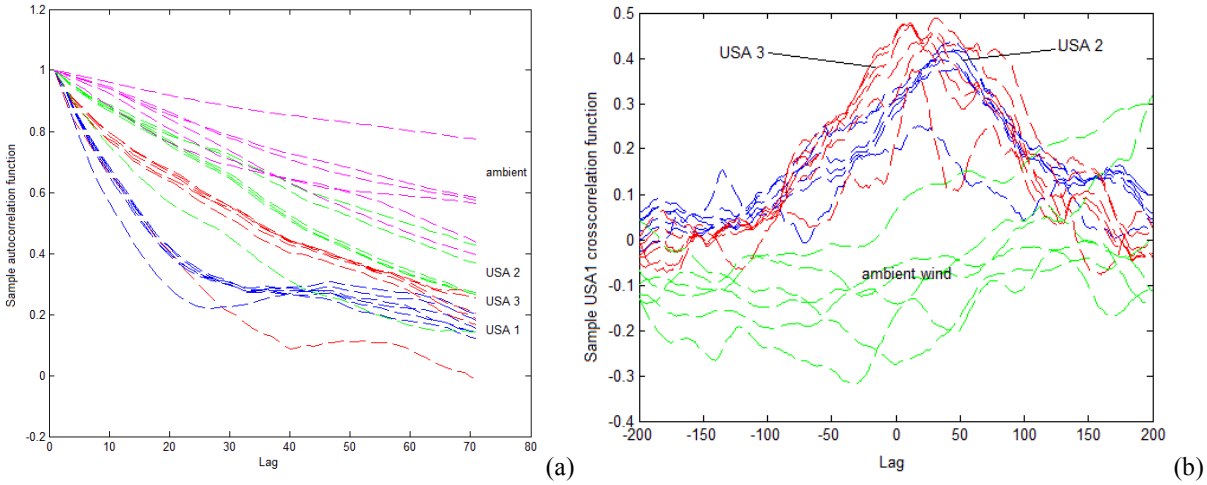

(a) (b)

Figure 9. Sub-process n°6/12: 12h00 to 14h00: (a) Sample autocorrelation functions of the single lane USA for multiple days realizations: USA 1 blue, USA 2 green, USA 3 red, ambient wind magenta; (b) Sample cross-correlation functions of USA 1 with USA 2 (blue), USA 3 (red) and ambient wind (green) for multiple days realizations. Refer to Figure 3 for USA numbering convention and geometry.

Frequency domain signal analysis is aimed at extracting the PSD of the daily traffic process, which is conveniently divided into 12 homogeneous sub-processes of 2 hours slice. Such hypothesis of circadian rhythm can be verified by a look at Figure 9-a, where multiple samples of different days (Monday to Friday population) show autocorrelation functions of the single lane USAs (see Figure 2 for numbering) that are generally less scattered than ambient wind USA. Furthermore USA 1, closest to top of truck, shows the narrowest band autocorrelation. Figure 9-b shows sample cross-correlation functions of the closest USA 1 to top of truck with other instruments of

the single-lane set: low coherence of the traffic induced turbulence with ambient wind results self-evident, while peaks and phase shifts in vertical upper USA 2 and lateral intermediate USA 3 positions (please refer to Figure 2 for USA numbering convention) tell us something about the three-dimensional structure of the separated wave induced by traffic. In fact, a high correlation and a minor shift with lateral intermediate position indicates possibly a proof for the experimental set-up assumption of the flow acting similarly in the 3.5m lane width as a whole; note also that symmetrical truck side edges vorticities can be considered in USA 1-USA 3 cross-correlation measurements, as the anemometers are placed symmetrically respect to central axis of truck (assumed to coincide with central axis of the lane, see Figure 2). Similarly, coherence of the three-dimensional structure of the wave can be assessed from the fact that in Figure 9-b cross-correlation peak with upper USA 2 is delayed from the peak of lower USA 3, closer to the wave source.

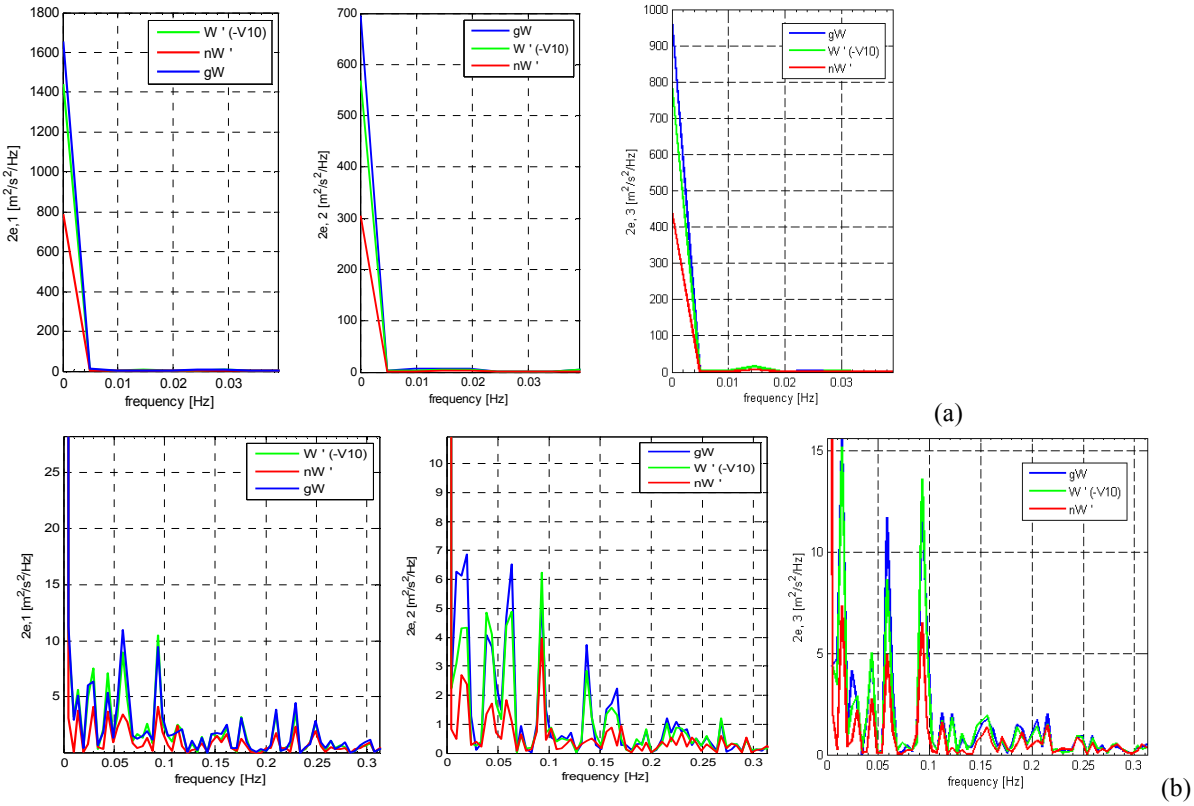

Figure 10. Sub-process n°6/12: 12h00 to 14h00: (a) PSD or 2e of USA 1, 2 and 3: detail of 0 Hz region of spectra; (b) PSD or 2e of USA 1, 2, and 3: detail of sub-Hertzian region of spectra. Each PSD contains three different signals transforms: gross wind (blue), turbulent wind (green), turbulent filtered wind (red).

Ergodicity assumption is also used to derive the PSD of the 12 sub-processes as the limit of the statistic mean:

$$\lim_{T\to\infty} E[\widetilde{PSD}_{\mathbf{gW-V_m}}(f)_T] = PSD_{\mathbf{gW-V_m}}(f) \tag{4}$$

where $\mathbf{gW - V_m}$ indicates the turbulent filtered signal. In fact, under the verified cyclostationary process assumption, one can take N days samples as N realizations, thus feeding equation (4) with:

$$\widetilde{PSD}_{\mathbf{gW}-\mathbf{V_m}}(f) = \frac{1}{N}\sum_{n=0}^{N-1}\frac{1}{T}\left|FFT\left(\mathbf{gW}-\mathbf{V_m}\right)_N\right|^2 \quad (5)$$

Pseudo spectral density of the absolute value of the turbulent wind vector can be seen as twice the relative TKE (see Equation 3). In Figure 10 are therefore presented the PSD or TKE of the single-lane anemometers set: detail is given to show both the 0 Hz and sub-Hertzian regions of the spectra containing energy. As the single vehicle passage has a main frequency widely above the sub-Hertzian region, the peak frequencies highlighted in Figure 10 can be typical of a certain regularity in the transit process, or to better say the slow separated wave of a column of trucks may be credited with.

6 CONCLUSIONS

It has been demonstrated that a 2D numerical approach is sufficiently accurate for a preliminary study of the drag coefficient and of the flow field related to the truck passing. Furthermore, flow structures above the truck have been successfully described. A direct link between the height of the separation bubble and the number of trucks has also been individuated both using CFD and experimental analysis.
In fact, results obtained from the motorway campaign have demonstrated good agreement with CFD simulations in reconstructing the wind velocity profiles for truck aerodynamic losses. In particular the contribute due to interaction between pressure wave, rear wake, and vehicles gap has proven to distinguish flow in high traffic density, and can be characterized by the proposed experimental set-up.

7 REFERENCES

[1] M.N. Albert. Field Testing of Cantilevered Traffic Signal Structures under Truck-Induced Gust Loads. MSc Thesis, University of Austin, Texas, May 2006.

[2] P.M. Cali and E.E. Covert. Experimental Measurements of the Loads Induced on an Overhead Highway Sign Structure by Vehicle-Induced Gusts. Journal of Wind Engineering and Industrial Aerodynamics, 84:87–100, April 2000.

[3] A.D. Quinn, C.J. Backer and N.G. Wright. Wind and Vehicle Induced Forces on Flat Plates - Part 2: Vehicle Induced Force. Journal of Wind Engineering and Industrial Aerodynamics, 89(9):831–847, April 2001.

[4] M. Ougburn, L. Ramroth and A.B. Lovins. Transformational Trucks: Determining the Energy Efficiency Limits of a Class-8 Tractor-Trailer. Rocky Mountain Institute Report, T08-08, July 2008.

[5] B.L. Storms, J.C. Ross, J.T. Heineck, S.M. Walker, D.M. Driver and G.G. Zilliac. An Experimental Study of the Ground Transportation System (GTS) Model in the NASA-Ames 7- by 10-ft Wind Tunnel. NASA Technical Memorandum, TM-2001-209621, February 2001.

[6] R.M. Wood and S.X.S. Bauer. Simple and Low-Cost Aerodynamic Drag Reduction Devices for Tractor-Trailer Trucks. SAE Technical Paper, 2003-01-3377, November 2003.

[7] C. Diebler and M. Smith. A Ground-Based Research Vehicle for Base Studies at Subsonic Speeds. NASA Technical Memorandum, TM-2002-210737 ,April 2002.

[8] K. Salari, J.M. Ortega and P.J. Castellucci. Computational Prediction of Aerodynamic Forces for a Simplified Integrated Tractor-Trailer Geometry. AIAA Fluid Dynamics Meeting, Portland, OR, United States, UCRL-CONF-204887, June 2004.

[9] C.J. Roy, J. Payne and M. McWherter-Payne. RANS Simulations of a Simplified Tractor/Trailer Geometry. ASME J. Fluids Eng., 128(5):1083 (7 pages), September 2006.

[10] S.P. Veluri, C.J. Roy, A. Ahmed, R. Rifki, J.C. Worley and B. Recktenwald. Joint Computational/Experimental Aerodynamic Study of a Simplified Tractor/Trailer Geometry. ASME J. Fluids Eng., 131(8):081201 (9 pages), August 2009.

[11] W.D. Pointer. Commercial CFD Code Validation for External Aerodynamics Simulations of Realistic Heavy-Vehicle Configurations. In "DOE Project on Heavy Vehicle Aerodynamic Drag FY 2005 Annual Report", UCRL-TR-217193, November 2005.
[12] D.G. Hyams, K. Sreenivas, R. Pankajakshan, D.S. Nichols, W.R. Briley and D.L. Whitfield. Computational Simulation of Model and Full Scale Class 8 Trucks with Drag Reduction Devices. Computers and Fluids, 41(1):27-40, February 2011.
[13] S. Maddox, K.D. Squires, K.E. Wurtzler and J.R. Forsythe. Detached- Eddy Simulation of the Ground Transportation System. In "The Aerodynamics of Heavy Vehicles: Trucks, Buses, and Trains." Lecture Notes in Applied and Computational Mechanics, Book 19. October 2004.
[14] S. Krajnović and L. Davidson. Development of Large-Eddy Simulation for Vehicle Aerodynamics. In: Proc. of IMECE2002, New Orleans, Louisiana, USA, IMECE2002-32833, November 2002.
[15] J. Östh. A LES Study of a Simplified Tractor-Trailer Model. Master's Thesis in Solid and Fluid Mechanics, Chalmers University Of Technology, 2010:34, 2010.
[16] F.M. White. Fluid Mechanics. McGraw-Hill, Fourth Edition, November 2002.
[17] N. Kalthoff, D. Baumer, U. Cosmeier, M. Kohler and B. Vogel, Vehicle Induced Turbulence near a Motorway, Atmospheric Environment, 39:5737-5749, 2005.
[18] A. V. Oppenheim, R. W. Schafer, J. R. Buck, Discrete-Time Signal Processing (2nd Edition) (Prentice-Hall Signal Processing Series), June 2011